AUTONOMOUS NAVIGATION OF SPACECRAFT FORMATIONSFOR ASTEROID EXPLORATION

Massimo Vetrisano[(1)] and Huixin Yang[(2)], Massimiliano Vasile[(1)], Weihua Zhang[(2)]
[(1)]*Advanced Space Concepts Laboratory, Department of Mechanical & Aerospace Engineering, University of Strathclyde. 75 Montrose Street G1 1XJ, Glasgow, UK, t:0141 548 2083, massimo.vetrisano@strath.ac.uk, massimiliano.vasile@strath.ac.uk* [(2)] *College of Aerospace Science and Engineering, National University of Defense Technology, Changsha, China, 410073.t:+44 07553462309, yang_huixin@yahoo.cn*

Abstract: This paper presents an autonomous multi-sensor navigation approach for a formation of spacecraft flying in the proximity of a near Earth asteroid.Each spacecraft embarks a different combination of high resolution cameras, attitude sensors and LIDAR to estimate the stateof each spacecraft in the formation. The work investigates the combination of measurements coming from multiple heterogeneous sensors and nonlinear sequential filtering technique to enable a formation to autonomously navigate in the proximity of asteroids.
This work is divided into two parts. Firstly, each spacecraft employs an Unscented Kalman Filter to data fuse multi-sensor measurements of the relative position of the spacecraft with respect to the asteroid possibly combined with measurements of the relative position of the spacecraft within the formation, thus determining position and velocity of each member. Secondly, the combination of the autonomous orbit determination with absolute measurements is considered. Absolute measurements include range and range rate measurements from the ground station and pseudo range rate measurements from on board Sun Doppler shift sensor. The combination of the two sets of measurements and state estimations from on-board and ground provides an interesting mean to accurately determine the orbit of asteroids.

Keywords: *multi-sensor, autonomous navigation, spacecraft formation, UKF, GNC, Near Earth Objects*

1. Introduction

Near Earth Objects (NEO), the majority of which are asteroids, are defined as any minor celestial object with a perihelion less than 1.3 AU and an aphelion greater than 0.983 AU. A subclass of these, deemed potentially hazardous asteroids (PHA), are defined as those with a Minimum Orbital Intersection Distance(MOID) from the Earth's orbit less than or equal to 0.05 AU and a diameter larger than 150 m. As of 10thOctober 2012, 9134 NEO's have been detected; of those, more than 2600 have a diameter larger between 0.3 and 1 km, and 1332 are listed as PHA[1]. Impacts from asteroids of about 1 km or more in diameter are considered to be capable of causing global climate change and destruction of ozone, with a land destruction area equivalent to a large state or country, while those with an average diameter of 100 m can cause significant tsunamis and/or land destruction of a large city. It is estimated that there are between 30000–300000 NEOs with diameters around 100 m, meaning a large number of NEOs are still undetected.
Different methods have been proposed and studied to deflect asteroids[2]. One interesting option is to use surface ablation with lasers or concentrated Sun-light. The use for

concentrated Sun-light was initially proposed by Melosh et al.[3] and envisioned a single large reflector; this idea was expanded in[4]to a formation of spacecraft orbiting in the vicinity of the NEO, each equipped with a smaller concentrator assembly capable of focusing the solar power at adistance around 1 km and greater. Vasile and Maddock[5]proposed to equip a multi-spacecraft system with a fibre laser and a solar concentrator. The main idea is to employ a swarm of spacecraft flying in the proximity of the asteroid with all the spacecraft beaming to the same location to achievethe required deflection thrust. They designed the formation orbits for the Earth-crossing asteroid Apophis 99942. Thefamily of asteroids, which Aphopis belongs to, comprised asteroids with semi-major axes larger than Earth (named after asteroid 1862 Apollo), where$a \geq 1$ AU, $r_p \leq 1.0167$ AU. Aphophis asteroid is seen as good representative of this class ofNEOs, with relatively low aphelion such that enough solar power can be harvested.

In order to accomplish such a mission, spacecraft formation must rely on a precise and reliable on board navigation system. The navigation in close proximity of asteroids can be complicated due to the fact the environment is relatively unknown and the dynamics is highly non-linear.

Usually spacecraft performs a close fly-by to estimate the gravitational harmonicsof the celestial minor bodies prior to operating near the asteroid itself. The knowledge of these figures is affected by uncertainty due to the way the fly-by is performed. Moreover, the asteroid could rotate, thus, making the trajectory subject to a perturbation, along with the solar radiation, which could render the trajectory unstable.This paper proposes and analyses different solutions to tackle this problem. A 2 spacecraft formation flying on the optimal trajectories generated in the previous work of Vasile and Maddock [5] is considered.

First of all, the dynamics model for the spacecraft evolution is introduced in Section 2. Since the evolution of the formation is such that the spacecraft could either impact the asteroid surface or leave the close proximity trajectory, a control strategy which allows keeping the actual trajectory close to the reference unperturbed case is required. For this purpose the dynamics includes the effect from a Lyapunov controller which is implemented for navigation purposes. Then Section 3 describes the measurements model and the decentralized systemwhich handles with different measurements and processes the information coming from the members of the formation by an Unscented Kalman Filter (UKF). Section 4analysed different measurements sets embarked on board to assess the on-board filtering capability. Finally, Section 5 shows that the asteroid's trajectory can be refinedand precise estimate can be obtained by including the measurements from the members of the formation.In this way it is possible to combine on-board measurements with the one coming from ground station during the deep space navigation prior asteroid approaching phases.

2. Dynamics Model and Filtering

The spacecraft in the formation are assumed to fly in formation with the asteroid, where the asteroid is at the centre of the local Hill's reference frame. Section 2.1 briefly introduces spacecraft's equation of motion in the relative frame, while Section 2.2 describes the implemented controller to maintain the trajectory.

2.1 Proximity motion and perturbations

In the proximity of the asteroid, in a Hill rotatingreference frame, the spacecraft are subject to the force due to solar pressure, the gravity of the asteroid, the gravity of the Sun, the centrifugal and Coriolis forces plus other forces induced by the impingement with the plume which are not considered in the followings.

It is here assumed that the asteroid is an ellipsoid with semi-axis a_I, b_I and c_I with c_I aligned with the z-axis of the asteroid Hill frame A in Figure1 and that the asteroid rotates around the z-axis with angular velocity w_a.

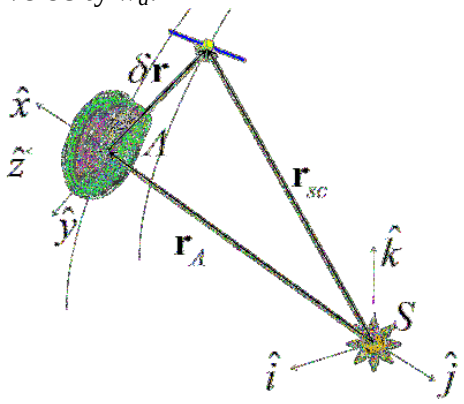

Figure1: Definition of the reference frames, including the rotating Hill frame A centred on the asteroid.

Assuming the asteroid's shape is an ellipsoid, the gravity field of the asteroid is expressed as the sum of a spherical field plus a second-degree and second-order field[6],

$$U_{20+22} = \frac{\mu_A}{\delta r^3}\left(C_{20}(1-\frac{3}{2}\cos^2\gamma) + 3C_{22}\cos^2\gamma\cos 2\lambda \right) \quad (1)$$

where the harmonic coefficients C_{20} and C_{22} are a function of the semi-axes

$$\begin{aligned} C_{20} &= -\frac{1}{10}(2c_I^2 - a_I^2 - b_I^2) \\ C_{22} &= \frac{1}{20}(a_I^2 - b_I^2) \end{aligned} \quad (2)$$

and γ is defined as

$$\lambda = \arctan(\frac{y}{x}) + w_A \quad (3)$$

If one considers a Hill reference frame centred in the barycentre of the asteroid, the motion of the spacecraft in the proximity of the asteroid itself is given by [7]:

$$
\begin{aligned}
\ddot{x} &= 2\dot{\nu}\left(\dot{y} - y\frac{v_{r_A}}{r_A}\right) + x\dot{\nu}^2 + \mu_{Sun}\left(\frac{1}{r_A^2} + \frac{r_A + x}{r_{Sc}^3}\right) + a_{Sun} - \mu_A\frac{x}{\delta r^3} + \frac{\partial U_{20+22}}{\partial x} + a_{w_x} \\
\ddot{y} &= -2\dot{\nu}\left(\dot{x} - x\frac{v_{r_A}}{r_A}\right) + y\dot{\nu}^2 - \mu_{Sun}\frac{y}{r_{Sc}^3} - \mu_A\frac{y}{\delta r^3} + \frac{\partial U_{20+22}}{\partial y} + a_{w_y} \\
\ddot{z} &= -\mu_{Sun}\frac{z}{r_{Sc}^3} - \mu_A\frac{z}{\delta r^3} + \frac{\partial U_{20+22}}{\partial z} + a_{w_z}
\end{aligned}
\tag{4}
$$

with

$$
\begin{aligned}
\ddot{\nu} &= -\frac{2v_{r_A}}{r_A}\dot{\nu} \\
\dot{v}_{r_A} &= \dot{\nu}^2 r_A
\end{aligned}
\tag{5}
$$

Note that the perturbations acting on the asteroid trajectory are assumed to be null and no effects such as solar radiation and spacecraft tugging is considered. The only perturbations modelled are the ones acting on the spacecraft. Beyond the gravitational perturbations from the asteroids, the major perturbation is due to the solar radiation, a_{Sun}, acting on the spacecraft along the x-axis

$$
a_{Sun} = C_R F_{Solar}(r_{Ssc})\frac{A}{m_{sc}} \tag{6}
$$

being A and m_{sc} the satellite cross section area and mass respectively, C_R the reflectivity coefficient and F_{Solar} the solar flux. Additional noise $\mathbf{a}_w = [a_{w_x} \quad a_{w_y} \quad a_{w_z}]$ is in the order of 10^{-9}m/s^2 , due to acceleration caused by the unbalanced attitude control manoeuvres. During the analysis an initial mass of about 500 kg and the maximum cross section area of about 20m^2 were considered. A mean value of 0.2 for the reflectivity coefficient is assumed. In general an uncertainty of 20% solar pressure is introduced as random noise.

As already mentioned in the introduction the spacecraft trajectories have been already designed and optimized in [5]. Table 1 reports the asteroid Keplerian elements along with its physical properties, which are assumed to be known during proximal motion.

Table 1: Orbital and physical properties of Aphophis

Element		Measured Value
Semi-major axis	a_A	0.9224 AU
Eccentricity	e_A	0.1912
Inclination	i_A	0.05814 rad
RAAN	Ω_A	3.5682 rad
Argument of periapsis	ω_A	2.2061 rad
Period	T_A	323.5969 d
Gravitational constant	μ_A	1.801599×10^{-9}km^3/s^2
Physical dimensions	a_l,b_l,c_l	191m, 135m, 95m
Rotational velocity	w_A	5.8177×10^{-5}rad/s

The results of the design process lead to define many suitable optimal trajectories. In the following analysis, 2spacecraft have been used. Their trajectories are given in terms of Keplerian elements variation with respect to the asteroid ones, as reported in Tab. 2.

Table 2: Initial spacecraft trajectory parameters variation with respect to the asteroid trajectory

	Parameter variation			
	$e[10^{-10}]$	$i[10^{-9}\text{deg}]$	$\Omega[10^{-8}\text{deg}]$	$\omega[10^{-8}\text{deg}]$
SC-1	-2.102	3.257	2.976	-4.318
SC-2	0.08913	3.828	5.370	-7.266

These orbits were designed to maintain the spacecraft close to the asteroid, reducing the requirements for control and allowing the spacecraft formation to point lasers on the same spot of the asteroid surface, reducing plumes contamination.

2.2 Lyapunov controller

Given these equations, the resultant of all the disturbing forces acting on the spacecraft is not zero. The combined effect from the gravitational field and the solar pressure is such that the spacecraft will either crash on the asteroid or diverge from a close proximity trajectoryTherefore, an active control is required to maintain the position of the spacecraft with respect to the asteroid.

If one assumes that centrifugal and Coriolis forces are negligible compared to solar pressure, gravity of the asteroid, and plume and that any non-spherical terms in the gravity field expansion result in only a small perturbation, then one can build a simple control law based on the Lyapunov control function:

$$V = \frac{1}{2}\delta v^2 + \frac{1}{2}K\left(\left(x - x_{ref}\right)^2 + \left(y - y_{ref}\right)^2 + \left(z - z_{ref}\right)^2\right) \quad (7)$$

where $\delta\mathbf{r}_{ref} = [x_{ref} \quad y_{ref} \quad z_{ref}]$ are the coordinates of a point along the nominal formation orbit (in the Hill frame). The assumption here is that the motion along the reference formation orbit is much slower than the control action. The necessary condition for the stability of the controller is that it must exist a controller $\mathbf{u}$ such that $dV/dt < 0$. Such a controller is defined as follows:

$$\mathbf{u} = -\left(\mathbf{a}_{Sun}(\delta\mathbf{r}) - \frac{\mu_A}{\delta r^3}\delta\mathbf{r}\right) - K\left(\delta\mathbf{r} - \delta\mathbf{r}_{ref}\right) - c_d\delta\mathbf{v} \quad (8)$$

If the actual trajectory of the spacecraft was known, the continuous control in Eq.(8) can now be introduced into the full dynamics model in Eqs.(4). Though, the trajectory is estimated by the navigation and in this way Eq.(8) becomes[8]:

$$\mathbf{u} = -\left(\mathbf{a}_{Sun}(\delta\mathbf{r}_{est}) - \frac{\mu_A}{\delta r_{est}^3}\delta\mathbf{r}_{est}\right) - K(t)\left(\delta\mathbf{r}_{est} - \delta\mathbf{r}_{ref}\right) - c_d(t)\delta\mathbf{v}_{est} \quad (9)$$

where $\delta\mathbf{r}_{ref}$, $\delta\mathbf{v}_{ref}$ are the estimated position and velocity from the filter and the two coefficients are time dependant, in order to account for the filter to converge, thus reducing

initial control.The elastic coefficient K was chosen to have $10^{-5}/s^2$ as steady value while the steady dissipative coefficient c_d was set to $10^{-4}/s$.

Once the controller along with the asteroid gravitational field is inserted in the spacecraft dynamics, one obtains a close loop problems in which control is performed together with estimation, and the filter equation has to consider the action of the controller itself. During the controlled phases it is assumed that the asteroid trajectory is known and, thus, the state variables to be estimated are the only ones related to the spacecraft formation.

An example of the combined filter process and the controller is reported in Figure2, where the initial condition for the analysis has seen an artificially perturbed trajectory of 10% in position with respect to the nominal unperturbed case and the trajectory was controlled for 10 days.

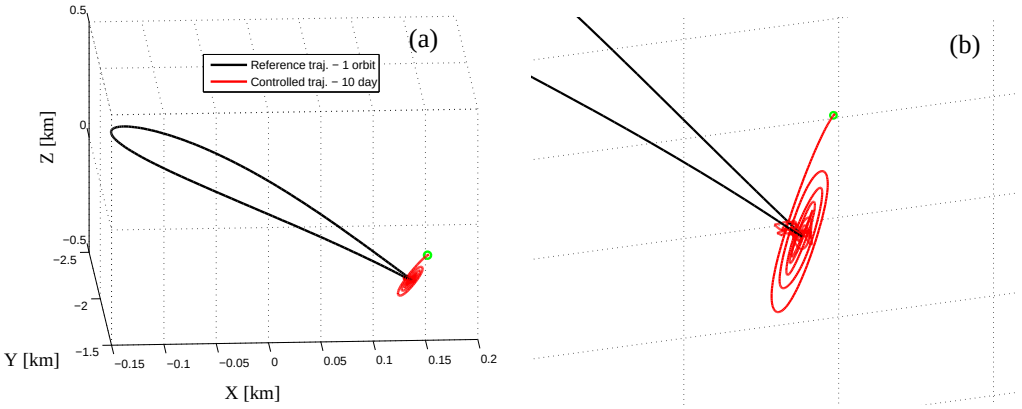

Figure2: (a) typical controlled and reference trajectories in the Hill reference frame, (b) close-up on the controlled trajectory for 10 days

Figure2(a) reports also the periodic trajectory in the Hill frame during the asteroid rotation period around the sun as obtained from [5]. At the beginning when deviations are high, the controlled trajectory presents a spiral trajectory typical of small thrust (Figure2(b)). Once the deviation has been reduced the spacecraft keeps on smalloscillations about the reference trajectory due to the combined effect from environment and controller itself.

2.3 The Unscented Kalman Filter

The unscented Kalman filter [9] works on the premises that by using a limited set of samples, optimally chosen, it should be easier to approximate a Gaussian distribution than to approximate a nonlinear function. The UKF was shown to be preferable to the Extended Kalmanfilter (EKF) in the case of nonlinear systems as the expected error in terms of mean and covariance matrix is lower, and it does not require the derivation of the Jacobian matrix[10].

3. Disaggregated Measurements Model and Data Fusion

Sections from 3.1to 3.5describe the model used for relative navigation along with the set of sensors used for improving the asteroid trajectory estimate. With reference to Figure3, these set is given by:

1. High resolution camera for elevation and azimuth in the spacecraft reference frame.

2. LIDAR/altimeter for obtaining the distance of the spacecraft from the asteroid surface.
3. Inter-satellite measurements which give relative elevation and azimuth angles along with relative distance between two spacecraft.
4. Range and range rate as seen from ground station.
5. Sun Doppler shift sensor, which descends from the radial velocity with respect to the Sun.

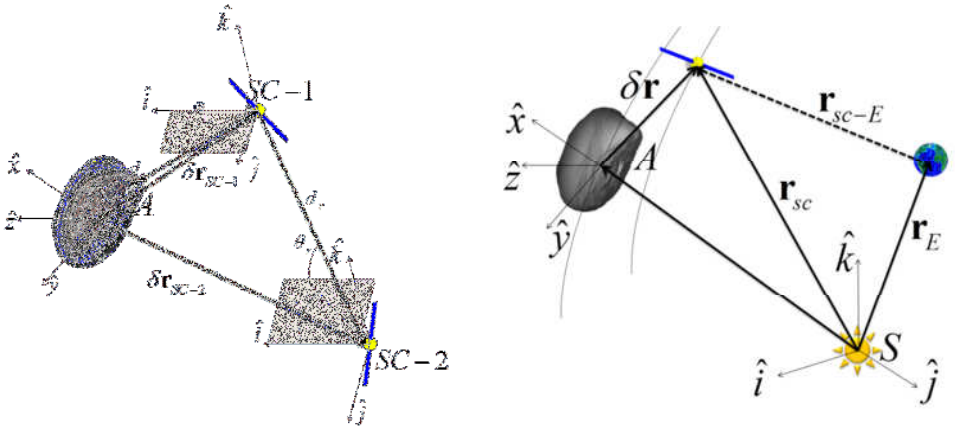

Figure3: Measurements model. (a) Relative navigation and (b) absolute navigation geometry.

After introducing the measurement model, section 3.6introduces the data fusion process, implemented to allow the filters to process all the data from the different spacecraft. Among these sensors, other sensors for the attitude estimation are embarked on board, e.g. sun sensors and star trackers. In this work the attitude of each spacecraft is assumed to be known with a level of precision corresponding to the precision of the star trackers. Furthermore, measuring the position of the Sun with respect to the asteroid and spacecraft could provide additional information, which can be used to generate a reasonable initial guess for the filters (i.e. to determine whether the spacecraft is in the positive or negative portion of the x-y plane in the Hill reference frame).

Table 3 summarizes the characteristic errors used in our analysis:

Table 3: Root square error in the diagonal elements of the error covariance matrix

Camera field-of-view	degree	30
Camera resolution	pixels	2048x2048
Camera focal length *f*	M	1.212×10^{-3}
Camera error	pixels	2
LIDAR range error	M	10
LIDAR pointing error	deg	10^{-3}
Inter-satellite range	M	2
Range	M	20
Range rate	mm/s	0.5
Doppler shift	mm/s	0.1
Angles/Attitude precision	deg	10^{-4}

We used conservative values for the ranging distances (reference [11] used a precision of 2 m for LIDAR), in order to simulate the surface roughness and asteroid's rotation. Angles on angular measurements and attitude are from [12]. Range and range rate are from[13] while we assumed a Doppler shift accuracy equal to the one used in[12]. The attitude precision on both axes is the same achieved by a star tracker.

3.1 Camera Model

The measurements from the camera are defined on the screen of the camera itself as the coordinates of the asteroid centroid and translated into angular measurements[11].

The definition of the asteroid as seen from the camera a certain number of points are taken the asteroid surface. With respect to Figure3, the position of each point is given in the spacecraft reference frame as:

$$\mathbf{x}^i_{Surf-SC} = \delta\mathbf{r}_{SC} - \mathbf{x}^i_{surface} \tag{10}$$

where $\mathbf{x}^i_{surface}$ are the position vectors of the points with respect to the centre of the asteroid. Then these points are given in the camera reference frame in the components $(x_{cam}, y_{cam}, z_{cam})^i$

$$\begin{aligned} x^i_{cam} &= \mathbf{x}^i_{Surf-SC} \cdot \mathbf{x}_{camera} \\ y^i_{cam} &= \mathbf{x}^i_{Surf-SC} \cdot \mathbf{y}_{camera} \\ z^i_{cam} &= \mathbf{x}^i_{Surf-SC} \cdot \mathbf{z}_{camera} \end{aligned} \tag{11}$$

where $\mathbf{x}_{camera}$, $\mathbf{y}_{camera}$ and $\mathbf{z}_{camera}$ represent the axes of the local camera frame. Being $\mathbf{v}^i = \begin{bmatrix} v^i_x & v^i_y & v^i_z \end{bmatrix}$ the normalized local vector, the position of the surface point in terms of pixel can be defined as:

$$\begin{aligned} x^i_{screen} &= v^i_x t_c \,/\, p_{width} \\ y^i_{screen} &= v^i_y t_c \,/\, p_{width} \end{aligned} \tag{12}$$

where $t_c = f \,/\, v^i_z$,f is the focal length and p_{width} is the pixel width. The centroid coordinates (x_c, y_c) is obtained by the mean position of the all points on the screen of the camera. A representation of this stage of the process is reported in Figure4which reports also the position of the centroid with respect to the actual centre.

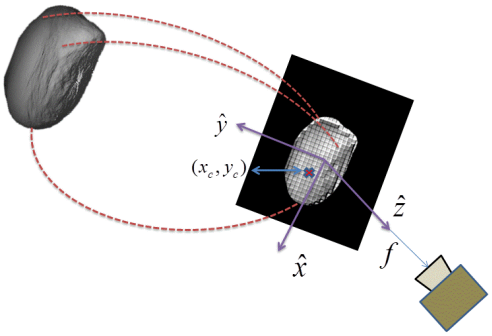

Figure4:Centroid identification

The local azimuth and elevation angles are obtained as:

$$\theta = \tan^{-1}\frac{x_c}{f} \qquad (13)$$
$$\varphi = \tan^{-1}\frac{y_c}{\sqrt{x_c^2 + f^2}}$$

The measurements from the camera are affected by both attitude and pixelization errors.

3.2 LIDAR

A minimum of two points on the asteroid surface is necessary to make navigation system observable. When a range measurement is added to a camera image, only one visible surface point is required for the navigation system to be observable[14]. LIDAR is a pulse laser which measures the travelling time of the pulse between the satellite and the asteroid. Here, we assume that the imaging landmark is the same as the point illuminated by LIDAR. The measurements from the LIDAR are given by the distance between the spacecraft and the spot the camera is pointing to along with LIDAR pointing angles:

$$d = \left|\mathbf{x}_{sc} - \mathbf{x}_{surface}\right| \qquad (14)$$

where $\mathbf{x}_{surface}$ is the position of the point the camera is pointing to on the asteroid surface. Angles are obtained as:

$$\varphi = \tan^{-1}\frac{y_c}{x_c} \qquad (15)$$

$$\theta = \tan^{-1}\frac{z_c}{\sqrt{x_c^2 + y_c^2}} \qquad (16)$$

This type of measurements is indirectly affected by camera error, which depends on the pixelization sensitivity and attitude, and directly by the characteristics error of the sensor, along with a bias defined by the mounting error of the instrument.

3.3 Inter-satellite measurements

The set of relative measurements is given by the distance between two spacecraft of the formation and local azimuth and elevation[15]. Being $\mathbf{d} = \begin{bmatrix} d_x & d_y & d_z \end{bmatrix}$ the distance array the measurements are given as following:

$$\begin{aligned} d &= \left| \delta \mathbf{r}_{sc1} - \delta \mathbf{r}_{sc2} \right| \\ \theta_r &= \tan^{-1} \frac{d_x}{d} \\ \varphi_r &= \tan^{-1} \frac{d_y}{d_x} \end{aligned} \tag{17}$$

where θ_r, φ_r are respectively the local azimuth and elevation. This type of measurements is indirectly affected by camera error, which depends on the pixelization sensitivity and attitude, and a bias defined by the mounting error of the instrument.

3.4 Earth range and range rate

The set of measurements defined by range, ρ , and range rate, $\dot{\rho}$, with respect to the ground station represents the typical set used to estimate spacecraft trajectory from Earth[13]and it is employed during deep space navigation. The rotation of the Earth is included in the model and this means that at a certain instant the measurements from ground cannot be available because the ground station navigation cannot point to the spacecraft.

3.5 Sun Doppler shift sensor

The Doppler shift from sun-light can be measured using aresonance-scattering spectrometer instrument which allows measuring the radial velocity of the spacecraft with respect to the Sun[12].The use of this kind of sensor is useful during the deep space navigation since could be used to integrate the relative and angular measurements from the spacecraft formation during the period in which the formation is not visible from ground.

3.6 Data fusion process

Each spacecraft of the formation receives the whole set of measurement coming from all the members and builds the necessary matrices, managing the reception of the available measurements. It must be considered that it has assumed that the measurements are received at the same time. Nonetheless at a certain stage of the simulation measurements could be unavailable. In fact the inter-satellite measurements could be unavailable because the sensors are blinded by the solar radiation. In this way the number of measurements is potentially different at each stage of the integration step.

This affects the forecasting and the updating stages, since it introduces inconsistency between the forecast measurements and the measurements that the system actually receives. The data fusion management can be described in a small number of process steps:

1. At the initial time t_0, an initial state vector and covariance matrix are assembled from the initial guess $\mathbf{x}_0^i$ and covariance $\mathbf{P}_0^i$ of each spacecraft ($i = 1 : N_{sc}$):

$$\mathbf{x}_0 = [\mathbf{x}_0^1 \quad \cdots \quad \mathbf{x}_0^{N_{SC}}]$$
$$\mathbf{P}_0 = \begin{bmatrix} \mathbf{P}_0^1 & & \varnothing \\ & \ddots & \\ \varnothing & & \mathbf{P}_0^{N_{SC}} \end{bmatrix} \tag{18}$$

2. At each time t_k, k=1,2…a set of measurements is received, a total array of measurements is assembled along with error covariance matrix using the available measurements $\mathbf{z}_k^i$ and instruments covariance error $\mathbf{R}_0^i$:

$$\mathbf{z}_k = [\mathbf{z}_k^1 \quad \cdots \quad \mathbf{z}_k^{N_{SC}}]$$
$$\mathbf{R}_k = \begin{bmatrix} \mathbf{R}_k^1 & & \varnothing \\ & \ddots & \\ \varnothing & & \mathbf{R}_k^{N_{SC}} \end{bmatrix} \tag{19}$$

   Based on the type of measurement the unperturbed set of equations $\mathbf{h_k}(\mathbf{x},t)$ is defined on the basis of the model introduced in Eqs. (12), (13), (14) and (17).
3. The UKF is then employed between the two instants ($t_{k,}$ t_{k+1}), obtaining the Kalman gain and the predicted state vector and measurements at time t_{k+1}.
4. At time t_{k+1} predicted and actual measurements are available.If the number of measurements is lower than the predicted number, only the consistent measurements between the two steps are considered in the update step. This is obtained either by removing the predicted measurements and the correspondent columns and rows in the Kalman gain or by giving a null value to the correspondent elements in the Kalman gain. If the number of actual measurements at time k+1 is higher than the one at the previous instant, then $\mathbf{R}_k$ and $\mathbf{h_k}(\mathbf{x},t)$ are consistently redefined and step from 2 to 4 are repeated.

4. Spacecraft formation navigation

The choice of sensors impacts the performance of the filter estimates and thus of the controllability of the system. In this section, 4 different cases have been considered:

- Case 1. Each spacecraft embarks a cameraand receives only range measurements from the LIDAR.
- Case 2. Each spacecraft embarks a cameraand receives range and angular measurements from the LIDAR.
- Case 3. The set of measurements from Case 2 is increased by including the inter-satellite range measurement.
- Case 4. The set of measurements defined in Case 3 is completed by inter-satellite azimuth and elevation angles.

Case 1 and Case 2 represent two cases in which the spacecraft are not collaborative and do not share information. On the contrary Case 3 and Case 4 feature collaborative spacecraft that share information.

Figure3shows the errors in position and velocity for each spacecraft embarking different sets of sensors and Table 4 reports the achieved errors at the end of the observation. An initial uncertainty of 10% in position and 1 mm/s in velocity with respect to the reference trajectory has been considered for all the analyses.

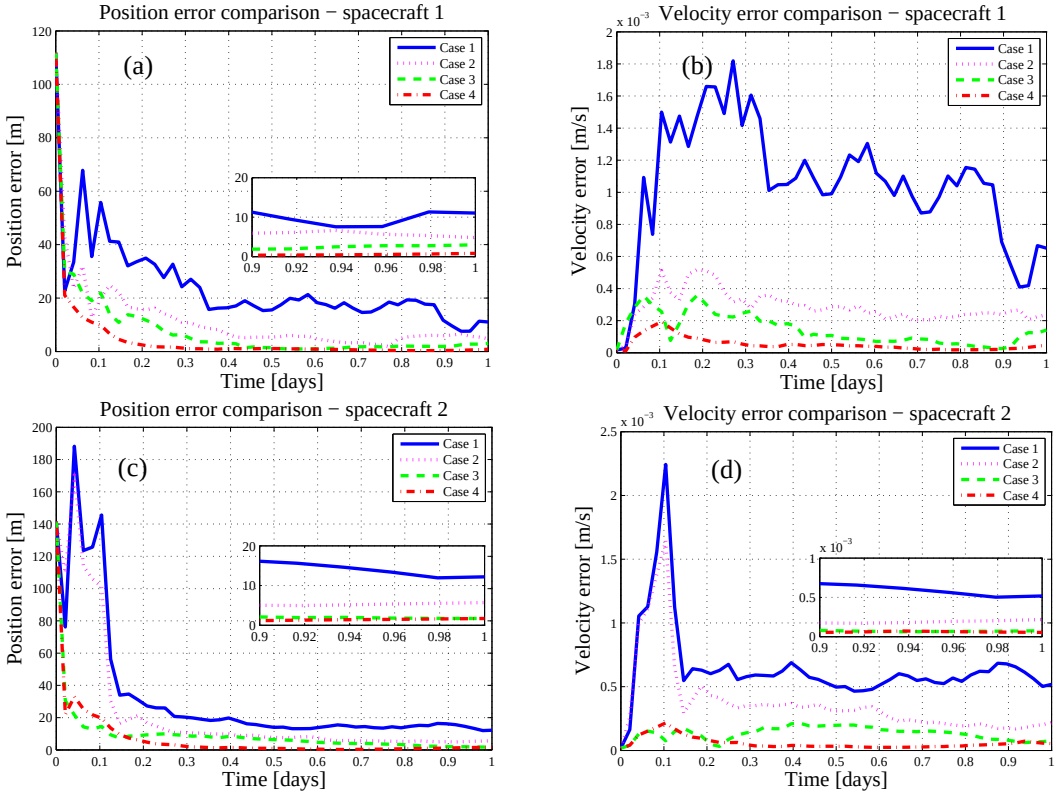

Figure5 : Comparison between different sensors set for spacecraft 1 (a),(b) and spacecraft 2 (c), (d)

Table 4 : Trajectory's estimated errors after 1 day

	Spacecraft 1		Spacecraft 2	
	Δr [m]	Δv[10^{-4}m/s]	Δr [m]	Δv[10^{-4}m/s]
Case 1	11.028	6.521	12.184	5.180
Case 2	4.800	2.357	5.715	2.176
Case 3	2.988	1.416	1.709	0.745
Case 4	0.814	0.485	1.699	0.542

As it can be seen, the non-collaborative cases are less precise than the collaborative ones. By including more measurements Case 2 results in being more precise than Case 1. A similar consideration is valid for the collaborative cases, where Case 4 achieves higher accuracy and a faster convergence than Case 3 by incorporating the inter-satellite angular measurements.

5. Asteroid trajectory refinement

During the deep space navigation phases, the on-board measurements can be employed in combination with the absolute measurements from the ground station to refine the trajectory of asteroids. In the following it is assumed the asteroid's trajectory is determined previously

by using local azimuth and elevation angles from ground observatories. Optical observations have been taken for a month before the spacecraft formation approaches the asteroid itself. Measurements obtained by considering the apparent magnitude to define pseudo range measurements could be included, but we considered only angular measurements. Angular measurements are more reliable since the surface reflectivity and asteroid's shape as well cannot be known precisely.

We assumed to have an Aphophis like trajectory as reference trajectory. The asteroid's state is estimated after 1 month optical observations with 1 hour sampling time. It has been assumed that the initial uncertainty in the asteroid's estimationis equal to 1% of the actual trajectory and angular measurements are as accurate as the one from a star tracker.

One can see from Figure6that after 1 month the errors can be more than 100 km in position and few cm/s in velocity.

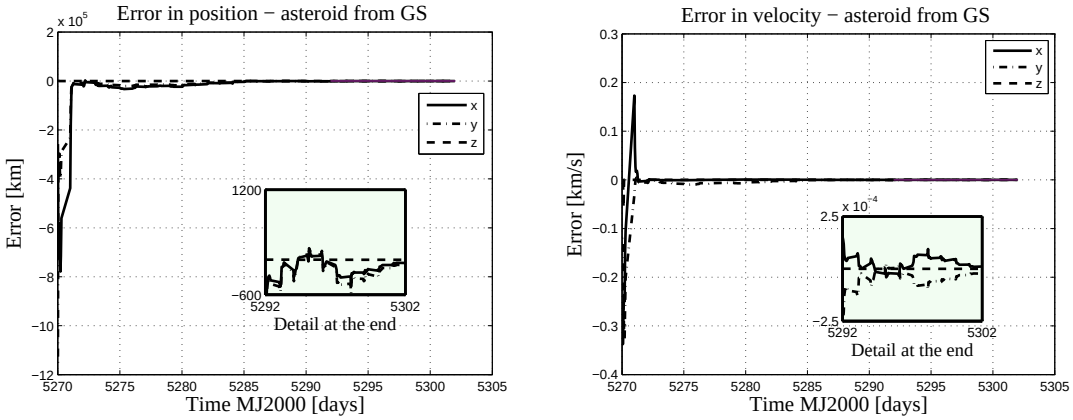

Figure6: Asteroid estimate error in 1 month optical observation from ground

If suitable navigation cameras with precision in the range of star tracker are employed combined to absolute measurements from the end of the optical ground station campaign and other on board instruments, the estimated asteroid state can be defined more accurately, as shown Figure7.

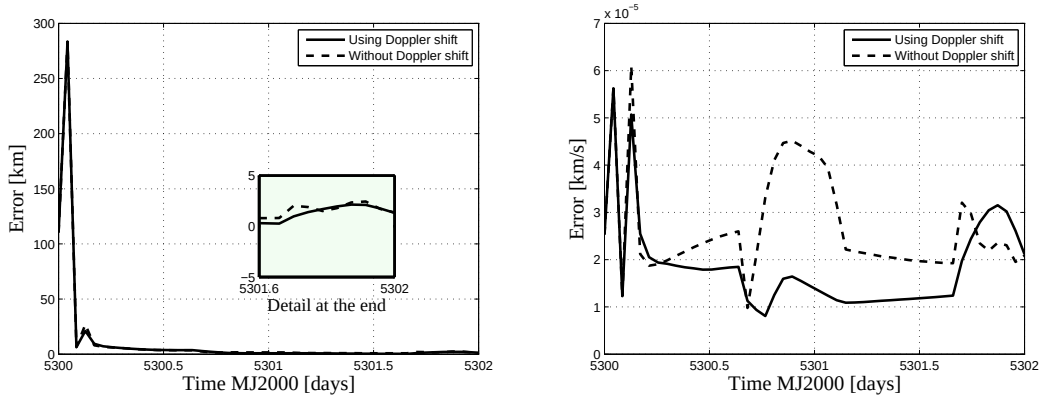

Figure7: asteroid estimate error in 2 days combined on board and ground station observation

The outcomes from the previous optical orbit determination, in terms of initial asteroid estimate and covariance matrix, have been included in the initial state estimate. The two spacecraft, spanned by about 10,000 km, are assumed to be travelling at a similar distance

from the asteroid at the beginning of the measurements acquisition. In order for the asteroid to be observable during the observation,its position does not have to be close to the line of sight of the two spacecraft. This condition is required because relative range from LIDAR cannot be used and it is not possible to state the position of the asteroid along the line of sight. The initial estimate for both spacecraft has been assumed to be known with an accuracy in position in the order of 1000 km and 0.1 m/s. We assumed that the ground station tracks both the spacecraft while one spacecraft embarks a Doppler shift sensor. The use of Doppler instrument has beneficial effects since it helps the filter converge toward lower error regions when ground station's tracking is not available. Peaks in the velocity error estimate are due to the unavailability of ground station measurements and only on-board sensors are employed.

The combined use of on board and ground station measurements allows improving the position estimate by approximately 2 orders of magnitude after 1 day, while the velocity estimate is not considerably improved.

6. Final remarks

This paper presented the navigation strategy for a small spacecraft formation in the proximity of the asteroid Aphophis. An Unscented Kalman filter has been implemented in order to data fuse the measurements from each spacecraft.

The disaggregate processing of the available measurements allows for higher flexibility as well asfor higher precision with respect to the single spacecraft data processing. A suitable data fusion technique has been used to deal with different sets of measurements at each time step. The analysis assesses the improvement of the localization performance of the navigation system by fusing the position information across 2 spacecraft with inter-satellite position information. The collaboration within the members of the formation increases the spacecraft navigation accuracy during the control phases. The results indicate that multi-sensor navigation can better solve the problem of the orbit determination of spacecraft formation in the proximity of near Earth asteroid.

Furthermore, the combined use of both on board and ground station measurements can be exploited to improve the asteroid trajectory estimate, in the case of short ground station observations. The improvement could be used to plan correction manoeuvres, thus approaching the asteroid with less propellant consumption. Another application could be to refine trajectories of PHAs' which the spacecraft could encounter during deep space navigation phases.

We are currently working a higher fidelity camera model able to deal with shaded parts, an improvement in the dynamics model which will include more gravitational harmonics as well as the perturbation due to the asteroid tugging and surface ablation. The interaction produces deviations in the nominal asteroid trajectory. This implies it will be also necessary to estimate the asteroid's trajectory during the formation proximal motion and operations.

7. References

[1] http:// neo.jpl.nasa.gov/stats

[2] Colombo, C., Sanchez Cuartielles, J. P., Vasile, M., Radice, G., October 2006. A comparative assessment of different deviation strategies for dangerous NEO. In: International Astronautical Congress. Valencia, Spain.

[3] Melosh, H. J., Nemchinov, I. V., Zetzer, Y. I., 1994. Non-nuclear strategies for deflecting comets and asteroids. In: Gehrels, T. (Ed.), Hazard due to comets and asteroids. University of Arizona Press, pp. 1111–1132.

[4] Maddock, C., Sanchez Cuartielles, J. P., Vasile, M., Radice, G., 2007. Comparison of single and multi-spacecraft configurations for NEA deflection by solar sublimation. In: Belbruno, E. (Ed.), New Trends in Astrodynamics and Applications III. Vol. 886. American Institute of Physics, pp. 303–316.

[5] Vasile, M. and Maddock, C.A., 2011: Design of a Formation of Solar Pumped Lasers for Asteroid Deflection, Preprint submitted to Advances in Space Research

[6] Hu, W. and Scheeres, D. J., July–August 2002. Spacecraft motion about slowly rotating asteroids. Journal of Guidance, Control and Dynamics 25 (4), 765–775.

[7] Schaub, H. and Junkins, J. L., 2003. Analytical mechanics of space systems, 1st Edition. AIAA Education Series. AIAA, Virginia, U.S.A.

[8] Vetrisano, M. and Vasile, M., 2012: Collaborative guidance navigation and control of disaggregated spacecraft in the proximity of minor bodies. In: 63rd International Astronautical Congress, Naples, Italy.

[9] Julier, J., Uhlmann, K. andDurrant-Whyte, H.F., 1995: A new approach for filtering nonlinear systems, Proceedings of the American Control conference, Seattle, Washington.

[10] Crassidis, J.L., Junkins, J.L.,2001: Optimal estimation of Dynamic Systems, S.Haykin, 2001.

[11] Dionne, K., 2009: Improving Autonomous Optical Navigation for Small Body Exploration Using Range Measurements. AIAA 2009-6106. AIAA Guidance, Navigation, and Control Conference, 10 - 13 August 2009, Chicago, Illinois

[12] Yim, J.R., Crassidis, J.L., and Junkins, J.L., 2000. Autonomous Orbit Navigation of Interplanetary Spacecraft. AIAA Guidance, Navigation, and Control Conference, Denver, CO, AIAA Paper 3936.

[13] Thornton, C. L. and Border, J.S., 2003: Radiometric Tracking Techniques for Deep-Space Navigation, JPL Deep Space Communications and Navigation Series, John Wiley & Sons Inc., Hoboken, New Jersey.

[14] Chung, L. R., 2006. Orbit determination methods for deep space drag-free controlled laser interferometry missions. Master thesis. University of Maryland.

[15] Alonso, R., Du, J.-Y., Hughes, D., Junkins, J.L., and Crassidis, J.L., 2001. Relative Navigation for Formation Flying of Spacecraft. Proceedings of the Flight Mechanics Symposium, NASA-Goddard Space Flight Center, Greenbelt, MD, pp. 115-129.